Numerical Heat Transfer, Part A: Applications: An International Journal of Computation and Methodology
Publication details, including instructions for authors and subscription information:
http://www.tandfonline.com/loi/unht20

The Numerical and Experimental Analysis of Heat Transport and Water Infiltration in a Granular Packed Bed Due to Supplied Hot Water

Phadungsak Rattanadecho [a], Seksan Suttisong [a] & Thitipan Somtawin [a]

[a] Center of Excellence in Electromagnetic Energy Utilization in Engineering (CEEE), Department of Mechanical Engineering, Faculty of Engineering, Thammasat University (Rangsit Campus), Pathumthani, Thailand

Published online: 14 Mar 2014.

To cite this article: Phadungsak Rattanadecho, Seksan Suttisong & Thitipan Somtawin (2014) The Numerical and Experimental Analysis of Heat Transport and Water Infiltration in a Granular Packed Bed Due to Supplied Hot Water, Numerical Heat Transfer, Part A: Applications: An International Journal of Computation and Methodology, 65:10, 1007-1022, DOI: 10.1080/10407782.2013.850969

To link to this article: http://dx.doi.org/10.1080/10407782.2013.850969

Numerical Heat Transfer, Part A, 65: 1007–1022, 2014

ISSN: 1040-7782 print/1521-0634 online
DOI: 10.1080/10407782.2013.850969

Taylor & Francis
Taylor & Francis Group

THE NUMERICAL AND EXPERIMENTAL ANALYSIS OF HEAT TRANSPORT AND WATER INFILTRATION IN A GRANULAR PACKED BED DUE TO SUPPLIED HOT WATER

Phadungsak Rattanadecho, Seksan Suttisong, and Thitipan Somtawin

Center of Excellence in Electromagnetic Energy Utilization in Engineering (CEEE), Department of Mechanical Engineering, Faculty of Engineering, Thammasat University (Rangsit Campus), Pathumthani, Thailand

The characteristics of heat transport and water infiltration in a granular packed bed due to supplied hot water are investigated experimentally and numerically. The distributions of water saturation and temperature are focused on one-dimensional models assuming the local thermal equilibrium between water and particles at any specific space in a vertical granular packed bed column. This study describes the dynamics of heat transport and water infiltration in various testing condition. The calculated water saturation, temperature distribution, and infiltration depth are compared with the experimental results. Experimentally and numerically, the influence of particle sizes and supplied water flux on heat transport during unsaturated flow are clarified in detail. The results showed that the granular packed bed with a larger particle size results in a faster infiltration rate and forms a wider infiltration depth. However, an extension of the heated layer is not as much as that of the infiltration layer because the temperature of water infiltration gradually drops due to upstream heat transport. It is found that a greater supplied water flux corresponds to a higher water saturation and temperature along a granular packed bed for each time increment. The numerical results closely match the experimental results.

1. INTRODUCTION

In the past few decades, the problem of heat transport in porous media or a granular packed bed with water infiltration due to capillary action is concerned with a variety of soil science, hydrology, agriculture, civil engineering, and chemical engineering applications, such as in temperature control of soil, recovery of geothermal energy, thermal energy storage, and various reactors in chemical industry. The infiltration of water is affected by several intrinsic and extrinsic factors. The intrinsic

Received 13 December 2012; accepted 17 September 2013.

Address correspondence to Phadungsak Rattanadecho, Center of Excellence in Electromagnetic Energy Utilization in Engineering (CEEE), Department of Mechanical Engineering, Faculty of Engineering, Thammasat University (Rangsit Campus), Pathumthani 12120, Thailand. E-mail: ratphadu@engr.tu.ac.th

Color versions of one or more of the figures in the article can be found online at www.tandfonline.com/unht.

NOMENCLATURE

c_p	specific heat, (J/kg.K)	u	velocity, (m/s)
d	particle diameter, (m)	ε	porosity, (m^3/m^3)
D_m	effective molecular mass diffusion [m^2/s]	ρ	density, (kg/m^3)
f	supplied water flow rate, $(kg/m^2)\cdot s$	λ	effective thermal conductivity, (W/ mK)
g	gravitational acceleration, (m/s^2)	μ	dynamics viscosity of liquid, (Pa s)
K	permeability, (m^2)	σ	surface tension, (N/m)
K_r	relative permeability		
p	pressure, (pa)	**Subscripts**	
q	heat flux, (W/m^3)	0	inlet, atmospheric
s	water saturation	1	first position
t	time, (s)	2	second position
T	temperature, (°C)	l	liquid phase

factors affecting the infiltration of water are the hydraulic conductivity function, water retention characteristics, and porosity of media. The extrinsic factors mainly refer to climatic conditions, such as water flow pattern, ambient temperature, water flow rate, and surface tension.

Until the present, the related problem of water infiltration in porous media has been investigated both experimentally and numerically by many researchers [1–7]. Pinder and Abriola [8] employed a finite difference approximation of the governing equations to describe non-aqueous phase liquid flow in the saturated zone. Celia and Binning [9] employed a finite element discrestization with fully implicit time stepping and Picard iteration to solve the air water flow equation. In order to consider flow phenomena, measurements were performed to visualize the flow pattern [10–14]. The computation analyses of heat and fluid flows have been studied by many researchers [18–20]. Although water infiltration processes have been studied actively for several decades, relatively few studies report the problem of heat transfer coupled with unsaturated flow in a granular packed bed systematically; especially, considering the effects of particle sizes and supplied water flux on transport phenomena with capturing infiltration depth have not been investigated before. In analysis of water infiltration, the governing equation is written in terms of the pressures in liquid phases through Darcy's equation in the mass balance equation. In analysis heat transport, the governing equation is written in terms of conduction and convection modes in the energy equation. This work is extended from the work of S. Suttisong and P. Rattanadecho [17] based on the work of our group (Aoki et al. [10]) and carried out in experimental and numerical work for analysis of heat transport and water infiltration in a granular pecked bed in several testing conditions. The purpose of this work is to study the influences of the particle size and supplied water flux on heat transport, water infiltration, and infiltration depth during unsaturated flow condition. The results presented here provide of a basis for a fundamental understanding of heat transport and unsaturated flow in porous media.

2. COMPUTATIONAL MODEL

By conservation of mass in the unsaturated porous media, the governing equation of infiltration flow can be derived by using the volume averaged technique [15, 16].

The main assumptions involved in the formulations of the transport model are as follows.

1. The unsaturated granular pack bed is rigid.
2. No chemical reactions occur in the granular packed bed.
3. Darcy's law holds for the liquid phase.
4. Gravity is included for the flow analysis.
5. Permeability of liquid can be expressed in terms of relative permeability.

Figure 1 shows the schematic diagram of a single-phase model or Buckley-Leverett problem. This is an unsaturated flow in a granular pack bed due to supplied water. The water is uniformly supplied at the top surface of the granular packed bed, which is initially composed of a glass particle and void with uniform porosity throughout.

In this study, it is noted that the supplied water flux during unsaturated flow is considered to be lower than the supplied water flux due to gravity (Aoki et al. [15]); namely,

$$f \leq g.k \tag{1}$$

Where f denotes supplied water flux, g denotes gravity, and k denotes saturated hydraulic conductivity (permeability). This expression means that the supplied water always infiltrates into granular packed beds throughout the infiltration process.

2.1. Mass Conservation

Regarding to infiltration flow in granular packed bed, the microscopic mass conservation equation for liquid flow in this packed bed is expressed as follows

$$\varepsilon \frac{\partial}{\partial t}[\rho_l s] + \frac{\partial}{\partial z}[\rho_l u_l] = 0 \tag{2}$$

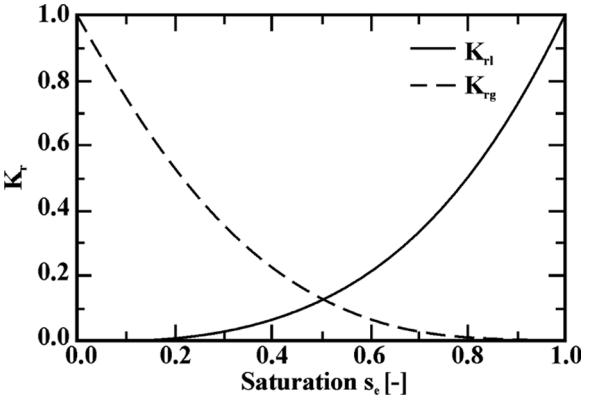

Figure 1. Relationship between K_r and s_e [16].

Where the generalized Darcy's law which is the expression for the superficial average velocity of the liquid phase, defined [15, 16] as follows.

$$u_l = -\frac{KK_{rl}}{\mu_l}\left[\frac{\partial p_g}{\partial z} - \frac{\partial p_c}{\partial z} - \rho_l g\right] \tag{3}$$

In Eq. (3), the capillary pressure, p_c, is related to the liquid and gas phases which can be written as follows.

$$p_c = p_g - p_l \tag{4}$$

Using Darcy's generalized equation (Eq. (3)), the mass conservation equation for a single-phase model (Eq. (2)) is then rewritten in its final form as follows.

$$\varepsilon\frac{\partial}{\partial t}[\rho_l s] - \frac{\partial}{\partial z}\left[\rho_l\frac{KK_{rl}}{\mu_l}\left(\frac{\partial p_g}{\partial z} - \frac{\partial p_c}{\partial z} - \rho_l g\right)\right] = 0 \tag{5}$$

Assuming the effect of gases pressure is negligible, the Eq. (5) is then reduced to:

$$\varepsilon\frac{\partial}{\partial t}[\rho_l s] + \frac{\partial}{\partial z}\left[\rho_l\frac{KK_{rl}}{\mu_l}\left(\frac{\partial p_c}{\partial z} + \rho_l g\right)\right] = 0 \tag{6}$$

2.2. Equilibrium Relations

The system of conservation equations obtained for Single-phase transport model require constitutive equation for relative permeabilities K_r, capillary pressure p_c, and capillary pressure functions (Brukley-Leverett functions) J. A typical set of constitutive relationships for liquid system is given by the following

$$K_{rl} = s_e^3 \tag{7}$$

Where s_e is the effective water saturation considered the irreducible water saturation, s_{ir}, and can be defined by the following.

$$s_e = \frac{s - s_{ir}}{1 - s_{ir}} \tag{8}$$

The relationship between relative permeability in liquid phase following Eq. (7) is shown in Figure 1.

The capillary pressure p_c is further assumed to be adequately represented by Brukley-Leverett's well know $J(s_e)$ functions. The relationship between the capillary pressure and the water saturation is defined by using Brukley-Leverett functions $J(s_e)$.

$$p_c = p_g - p_l = \frac{\sigma}{\sqrt{K/\varepsilon}}J(s_e) \tag{9}$$

Where $J(s_e)$ is correlated capillary pressure data obtained by Brukley-Leverett and can be expressed as follows [15, 16].

$$J(s_e) = 0.325(1/s_e - 1)^{0.217} \tag{10}$$

2.3. Initial Condition and Boundary Conditions for Mass Transfer Analysis

Assuming that the initial effective water saturation and initial temperature are constant and uniformed throughout the granular packed bed,

$$t = 0,\ z \geq 0 : s_e = s_0,\ \ T = T_0 \tag{11}$$

Based on experimental conditions, the initial effective water saturation s_0 is given as $s_0 = 0.001$ and the initial temperature T_0 is given as $T_0 = 25$ [°C]. The boundary conditions at the top and the bottom sides of granular packed bed are as follows.

$$\begin{aligned} &t > 0,\ z = 0 :\ F_{l,in} = const \\ &z = L :\ F_{l,out} = \rho_l\ u_l \end{aligned} \tag{12}$$

2.4. Energy Conservation

Ignoring kinetic energy and pressure terms which are usually unimportant, this can be obtained from the total energy conservation of combined solid and liquid phases and by invoking the assumption that the local thermodynamic equilibrium prevails among all volume. The temperature of the sample during unsaturated flow due to supplied hot water is obtained by solving the conventional heat transport equation.

$$\frac{\partial}{\partial t}\left[\left(\rho c_p\right)_T\right] + \frac{\partial}{\partial z}\left[\left(\rho_l c_p u_l\right)T\right] = \frac{\partial}{\partial z}\left[\lambda \frac{\partial T}{\partial z}\right] \tag{13}$$

Where $(\rho c_p)_T$ is the effective heat capacitance of porous layered, and λ is the effective thermal conductivity depending on water saturation. Under thermal equilibrium conditions and using the volume average technique, the effective heat capacitance is given by the following.

$$\left(\rho c_p\right)_T = \rho_l c_{pl} \varepsilon s + \rho_p\ c_{pp}(1 - \varepsilon) \tag{14}$$

Based on the experimental results [15, 16] using glass beads saturated with water, the effective thermal conductivity is represented as a function of the water saturation.

$$\lambda = \frac{0.8}{1 + 3.78e^{-5.95s}} \tag{15}$$

2.5. Initial Condition and Boundary Conditions for Energy Analysis

Assuming that the initial effective water saturation and initial temperature are constant,

$$t = 0,\ z \geq 0 :\ s_e = s_0,\ \ T = T_0 \tag{16}$$

From experimental conditions, initial effective water saturation s_0 is given as $s_0 = 0.001$ and the initial temperature T_0 is given as $T_0 = 25$ [°C]. The boundary conditions at the top and the bottom sides of porous layered are as follows.

$$t > 0,\ z = 0:\ F_{l,in} = const, \quad q_{l,in} = \rho_l c_{pl} u_l T_{in} \tag{17}$$

2.6. Numerical Schemes

Corresponding to the method of finite differences based on the notion of control volumes, the generalized system of nonlinear equations are integrated over typical rectangular control volumes. After integrating over each control volume within computational mesh, a system of nonlinear equations result whereby each equation within this system can be cast into a numerical discretization of the generalized conservation equation. The equations of heat transport and unsaturated flow are nonlinear because p_c and K_{rl} depend on s. To solve the nonlinear equations the Newton-Raphson iteration procedure are used for each grid. The single-phase model (Eq. (6)) for the internal nodes can be cast into a numerical discretization as follows.

$$\begin{aligned} &\frac{\varepsilon}{\Delta t}(1 - s_{ir})\left(\rho_l(s_{ei}^{n+1} - s_{ei}^{n})\right) \\ &+ \quad \frac{1}{\Delta z}\left(\rho_l\left(\frac{KK_{rl}}{\mu_l}\bigg|_{i+\frac{1}{2}}\left(\frac{P_{ci+1}^{n+1} - P_{ci}^{n+1}}{\Delta z} + \rho_l g_z\right)\right.\right. \\ &\quad \left.\left. - \frac{KK_{rl}}{\mu_l}\bigg|_{i\frac{1}{2}}\left(\frac{P_{ci}^{n+1} - P_{ci-1}^{n+1}}{\Delta z} + \rho_l g_z\right)\right)\right) = 0 \end{aligned} \tag{18}$$

The discretized form of the heat transport equation (Eq. (13)) is given by the following

$$\begin{aligned} &\frac{\left(\rho C_p\right)_{Ti}^{n+1} T_i^{n+1} - \left(\rho C_p\right)_{Ti}^{n} T_i^{n}}{\Delta t} + \frac{\rho_l C_{pl}}{\Delta z}\left(u_{li}^{n+1} T_i^{n+1} - u_{li-1}^{n+1} T_{i-1}^{n+1}\right) \\ &- \frac{1}{\Delta z}\left(\lambda_{i+\frac{1}{2}}^{n+1}\left(\frac{T_{i+1}^{n+1} - T_i^{n+1}}{\Delta z}\right) - \lambda_{i-\frac{1}{2}}^{n+1}\left(\frac{T_i^{n+1} - T_{i-1}^{n+1}}{\Delta z}\right)\right) = 0 \end{aligned} \tag{19}$$

The grid convergence index (GCI) has been used to estimate the uncertainties of grid-spacing for the fine grid solution, which is expressed as follows [21, 22].

$$GCI_{fine}^{21} = \frac{1.25\left|e_a^{21}\right|}{r_{21}^{p} - 1} \tag{20}$$

$$p = \frac{\ln(e_{32}/e_{21})}{\ln(r)} \tag{21}$$

$$e_a^{21} = \left|\frac{\phi_1 - \phi_2}{\phi_1}\right| \tag{22}$$

Where GCI is grid uncertainty, e_a^{21} is approximate relative error, r is refinement ratio, p is apparent order, $e_{32} = \phi_3 - \phi_2$, $e_{21} = \phi_2 - \phi_1$, ϕ_1, ϕ_2, and ϕ_3 is solutions

for the fine, medium, and coarse grids, respectively. The convergence test carried out using GCI with grid numbers of 80, 40, and 20. These grid numbers represent the coarse, medium, and fine grids with spacing 0.02, 0.01, and 0.005 meters, respectively. The solutions for the fine, medium, and coarse grids are 29.2771, 28.7308, and 27.3773, respectively. From the calculation in Eqs. (20–22), the apparent order is 1.31, the approximate relative error is 1.87%, and the numerical uncertainty in the fine-grid solution is 1.58%. It is reasonable to assume that, at this number of grid, the accuracy of the simulation results is independent from the number of grid for all simulation. This takes 1–5 min on work stations with a dual-core processor (1.73 GHz) and 1 GB of RAM.

3. EXPERIMENTAL APPARATUS

Figure 2 shows the experimental apparatus for one-dimensional heat transport and water infiltration in granular packed bed. The test column is designed to achieve one-dimensional infiltration flow and heat transport. The test column constructed with inner diameter of 60 mm and 400 mm long column is made of rigid acrylic plastic tubing. The dry porous-ceramic disk at the bottom of the granular packed bed supported the granular particles in the column while allowing a way for air to escape in advance of infiltration depth. Each test column is radially insulated to minimize heat loss through the column walls. A thick plug of insulation is also placed again the ceramic disk of the bottom of column to minimize axial heat loss.

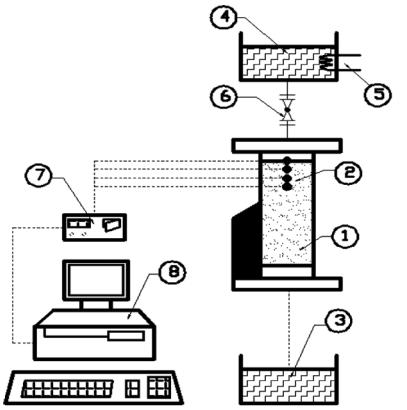

1. Granular packed bed 2.Thermocouples

3. Water tank 4.Hot water tank

5. Heater 6.Control valve

7. Recorder 8.Computer

Figure 2. Experimental apparatus for measuring heat transport and water infiltration in a granular packed bed.

The radial insulation made the columns effectively one-dimensional with respect to heat transfer. Spherical soda lime glass beads with average sizes (d) of 0.15 and 0.4 mm. are used as a sample of granular packed bed. The final assembly thus provided for packing glass beads in the test column with the thermocouples on the axis of the column. The hot water is supplied (supplied water flux, f) from a tank is heated at a certain temperature (T_s) to the top of granular packed bed through a distributor. The hot water supply is controlled by a control valve, where the water flux is calculated from the measured volume used over a period of time. The temperature distributions within test columns are measured with Cu-C thermocouples with diameter of 0.1 mm. These thermocouples are inserted to approximately the center line with 20 mm interval along the vertical axis of test column. The distributions of temperature are recorded by a data logger connected to a computer.

Figure 3 shows the experimental apparatus for measuring water saturation. The position of infiltration depth in the packed bed is captured by digital camera relative to a time-base reference, as shown in Figure 4. At the end of test run, the granular packed bed is cut out into five sections in small volume of 183 cm^3 in order to measure the water saturation. The water saturation in the non-hygroscopic porous packed bed was defined as the fraction of the volume occupied by water to volume of the pores. This water saturation was obtained by weighing dry and wet mass of the sample. Before the experiment, each section was weighed individually to record its dry mass. The porous packed bed was weighed again at 5 and 10 min after the test run. The water saturation formula can be described in the following form [16]:

$$s = \frac{\rho_p \cdot (1 - \varepsilon) \cdot (m_w - m_d)}{\rho_w \cdot \varepsilon \cdot m_d} \tag{23}$$

(a)

(b)

Figure 3. Experimental apparatus for measuring water saturation in a granular packed bed: (a) Weighing scales and (b) the five sections of granular packed bed.

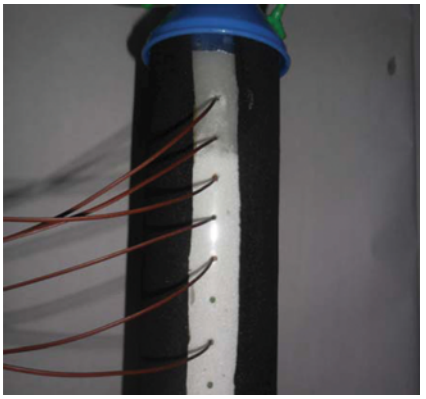

Figure 4. Experimental apparatus for measuring infiltration depth of water.

Where s is water saturation, ρ_p is density of particle, ρ_w is density of water, ε is porosity, and m_w and m_d are wet and dry mass of the sample, respectively.

Initially, the water saturation and the temperature are uniformed within packed bed are 0.06 and 25°C, respectively. The experiments are carried out for the conditions of constant supplied water flux and constant temperature of hot water.

During the experiments, the uncertainty of the data might be due the variations in humidity, room temperature, and human errors. The calculated uncertainties in all tests are less than 2.85%. Additionally, a possible error in the predicted results might be due to the uncertainties in the calculated effective thermal conductivity and the permeability of the porous media.

4. RESULTS AND DISCUSSION

This study described the dynamics of heat transport and water infiltration in various testing condition. The calculated water saturation, temperature distribution, and infiltration depth are compared with the experimental results. Experimentally and numerically, the influences of particle sizes and supplied water flux on heat transport during unsaturated flow are clarified in details. The particle sizes used in this work are 0.15 mm and 0.40 mm in diameter, supplied water fluxes are 0.05 kg/m^{2}s and 0.1 kg/m^{2}s and supplied water temperature is controlled at 55°C and the initial temperature T_0 is given as $T_0 = 25$°C.

The experimental and numerical analysis of heat transport and water infiltration in granular pecked bed in several testing condition are shown in Figures 5–7. Figure 5 shows water saturation at various elapsed times, which corresponds to the diameter of 0.15 mm and supplied water flux of 0.1 kg/m^{2}s. It is found that the experimental results fairly match with numerical results. At elapsed time, the water saturations form wider infiltration layer where the capillary action and gravitational force play an important role on water infiltration process. Figure 6 shows the numerical results for the temperature distributions are in agreement with the experimental results. The temperature distribution at 10 min forms wider and deeper than the temperature distribution at 5 min. The heat conduction and convection from hot water infiltration play an important role on heat transport

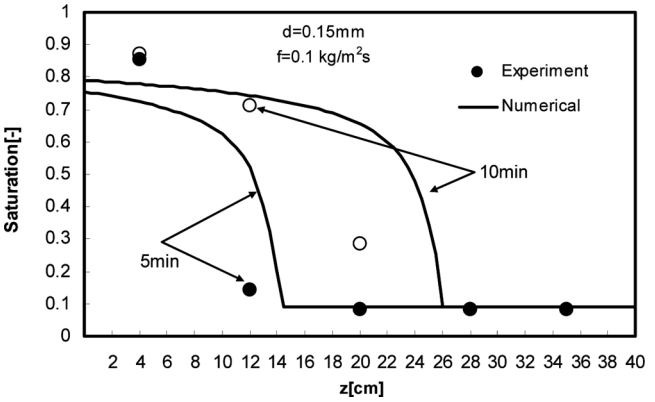

Figure 5. Numerical results of water saturation with the supplied water fluxes 0.1 kg/m^{2}s at 5 and 10 min compared with the experimental results. ($d = 0.15$ mm, and supplied water temperature $T_s = 55$°C.)

phenomena. However, an extension of the heat layer (Figure 6) is not as much as that the infiltration layer (Figure 5). For the infiltration depth, the experimental results is closely match with numerical results, as shown in Figure 7, with supplied water flux of 0.1 kg/m^{2}s and particle size of 0.15 mm.

Figure 8 shows the distributions of water saturation and temperature at various elapsed times as a parameter of supplied water flux, which corresponds to the diameter of 0.15 mm. It is found that a greater supplied water flux in the packed bed corresponds to higher water saturation and forms a wider infiltration layer. The numerical results are in agreement with experimental results. Here, the main transport mechanism that enables water infiltration in granular packed bed is by capillary pressure gradient and gravity. Liquid phase migration is related to capillary pressure gradient as well as temperature (which correspond to that of surface tension, as referred to in Eq. (9). The temperature in the granular packed bed rises

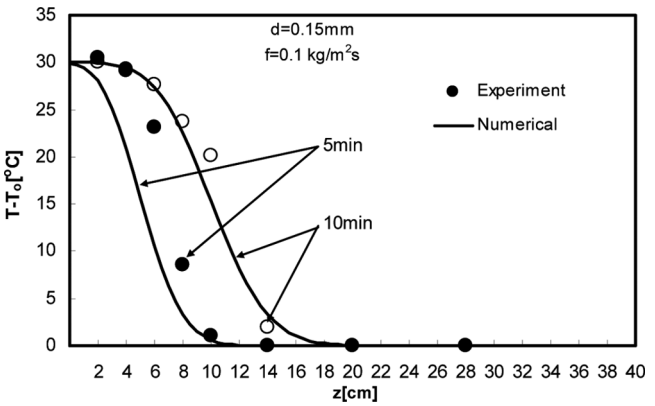

Figure 6. Numerical results of temperature distribution along a granular packed bed with the supplied water fluxes 0.1 kg/m^{2}s at 5 and 10 min compared with the experimental results. ($d = 0.15$ mm, and supplied water temperature $T_s = 55$°C.)

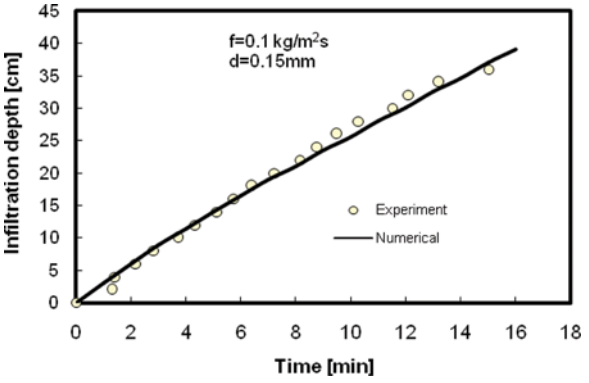

Figure 7. Numerical results of infiltration depth along a granular packed bed with the supplied water fluxes 0.1 kg/m^{2}s, with respect to elapsed times compared with the experimental results ($d = 0.15$ mm, and supplied water temperature $T_s = 55$°C.).

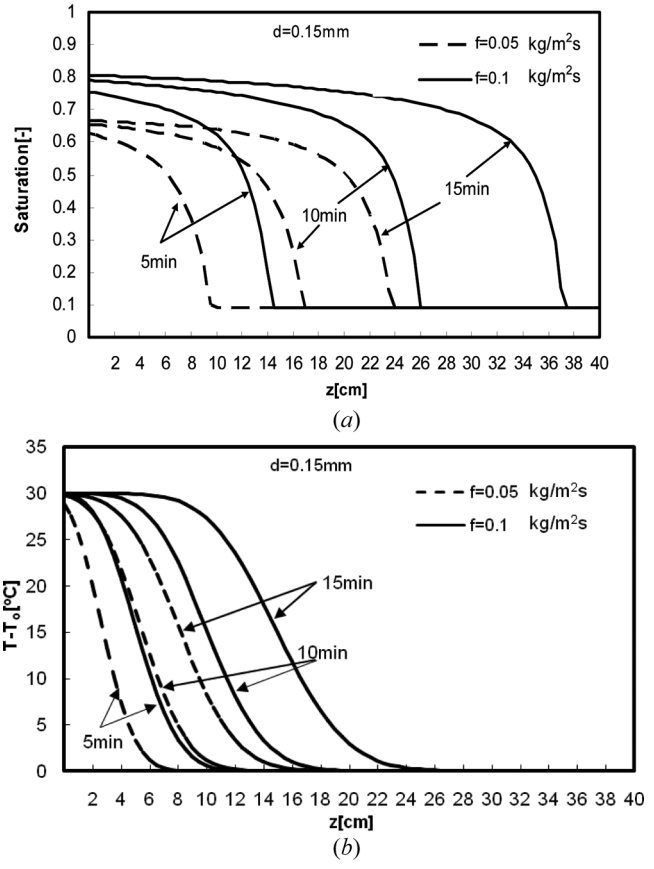

Figure 8. Numerical results of (*a*) temperature profiles and (*b*) water saturation along a granular packed bed with the supplied water fluxes 0.05 kg/m^{2}s and 0.1 kg/m^{2}s with respect to elapsed times. ($d = 0.15$ mm, and supplied water temperature $T_s = 55$°C.)

due to water infiltration, but the heated layer does not extend as much as the infiltration layer similarly explained in previous figures. Figure 9 shows the distributions of water saturation and temperature at various elapsed times as a parameter of particle size, which corresponds to the supplied water flux of 0.05 kg/m^{2}s. In Figure 9*a*, it is found that using the larger particle size results in lower water saturation but it penetrates much deeper than that of the smaller particle size at each time instant. This is because the larger particle size and hence pore size of these particles reduces the capillary pressure to resist a gravity driven during water infiltration process. In Figure 9*b*, it is found that the temperature distributions of both particle sizes taken at the early stage show nearly the same tendency, that is the temperature decreases to low values within short distance. While in the later stages, the significantly different temperature between the two particles sizes occurs over an infiltration layer. This is because the permeability of the porous medium, as well as the capillary pressure, becomes the strongly dominant factor to the water infiltration and heat transfer in the granular packed bed for the approached steady

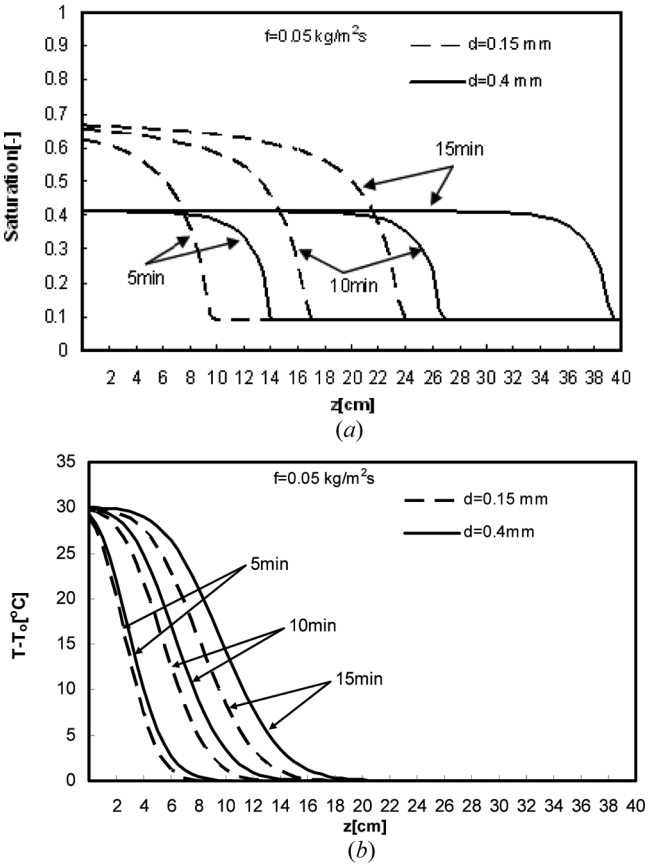

Figure 9. Numerical results of (*a*) temperature profiles and (*b*) water saturation along a granular packed bed with the particle sizes 0.15 and 0.4 mm with respect to elapsed times. (Supplied water flux $f = 0.05$ kg/m^{2}s, and supplied water temperature $T_s = 55$°C.)

state infiltration process. The result shows that a larger particle size leads to faster infiltration rate and forms a wider infiltration layer corresponds to the experimental results.

Figure 10 shows the infiltration depth in a granular packed bed at various elapsed times. The infiltration depth of higher supplied water flux displays a deeper than the infiltration depth of lower supplied water flux, as shown in Figure 10*a*. This figure shows the influence of particle sizes on the distributions of saturation and temperature with respect to elapsed times under the same particle sizes of 0.15 mm with different supplied water flux (0.05 kg/m^2s and 0.1 kg/m^2s). The effect of particle size on infiltration depth is also clearly shown in Figure 10*b*. This figure shows the infiltration depth with respect to elapsed times of the packed bed as a parameter of particle sizes (0.15 mm and 0.4 mm) at supplied water flux of 0.05 kg/m^2s. It is found that the infiltration depth of the larger particle size displays

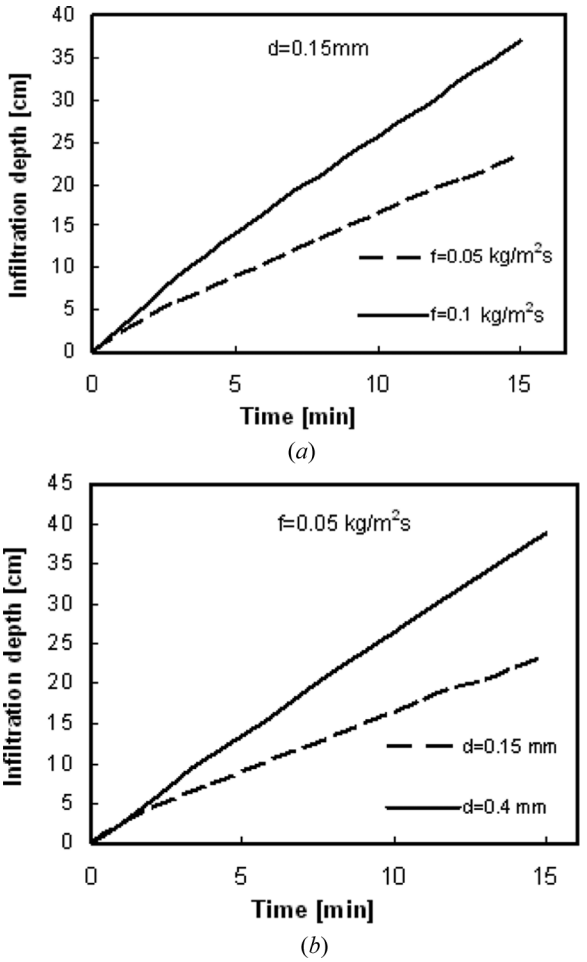

Figure 10. Numerical results of (*a*) infiltration depth as a parameter of supplied water flux and (*b*) particle size along a granular packed bed with respect to elapsed times.

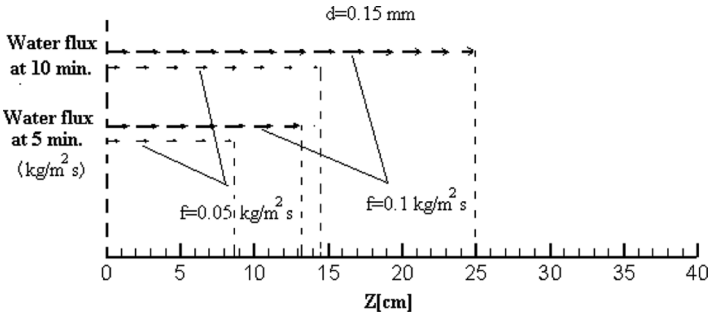

Figure 11. Vectors of water fluxes as a parameter of supplied water flux along a granular packed bed at 5 and 10 min. ($d = 0.15$ mm, $f = 0.05$, and 0.1 kg/m^{2}s.)

a deeper than the infiltration depth of smaller particle size, due to the effect of the hydrodynamic characteristics (Capillary pressure and gravity). Next, the water fluxes flow (vector profiles) will be presented in figures 11 and 12, where it is obtained from numerical results. Figure 11 shows the vectors of water fluxes as a parameter of supplied water flux at 5 and 10 min. As shown in Figure 11, it is found that at 5 min, the infiltration depth of the water flux vectors are 14 cm and 9 cm for the supplied water fluxes of 0.1 kg/m^{2}s and 0.05 kg/m^{2}s, respectively. While at 10 min, the infiltration depth of the water flux vectors are 25 cm and 10 cm for the supplied water fluxes of 0.1 kg/m^{2}s and 0.05 kg/m^{2}s, respectively. This is attributed to the presence of a higher volumetric body force of higher supplied water flux (0.1 kg/m^{2}s) that accelerated a faster water flux than that of 0.05 kg/m^{2}s. Figure 12 shows the vectors of water fluxes as a parameter of particle size at 5 and 10 min, with the water flux at the surface of 0.1 kg/m^{2}s. As shown in Figure 12, it is found that at 5 min, the infiltration depth of the water flux vectors are about 15 cm and 13 cm for the particle size of 0.4 mm and 0.15 mm, respectively. While at 10 min, the infiltration depths of the water flux vectors are about 35 cm and 25 cm for the particle size of 0.4 mm and 0.15 mm, respectively. From the results, the magnitudes of water flux vectors near the surface of the packed bed are found to be higher than that of the infiltration front region. This is because the water saturation is higher near the surface of the

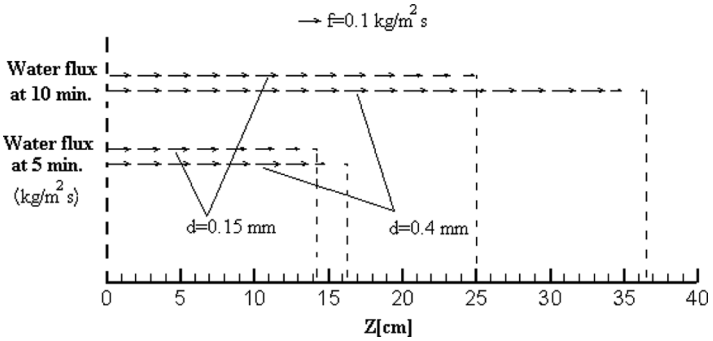

Figure 12. Vectors of water fluxes as a parameter of particle size along a granular packed bed at 5 and 10 min. ($f = 0.05$ kg/m^{2}s, $d = 0.15$, and 0.4 mm.)

packed bed, and at the infiltration front region where the water saturation is low resulting in the different magnitude of the relative permeability, as shown in Figure 1.

5. CONCLUSION

The heat transport and water infiltration in granular packed bed with unsaturated flow is investigated numerically and experimentally. The following are the conclusions of this work.

1. The heat transport hardly occurs in the layer close to the infiltration front because the temperature of water infiltrating gradually drops due to heat transport upstream. Furthermore, the effect of particle size on the discrepancy of heated layers is smaller compared to that of the water infiltration layers.
2. It is found that the gravity and capillary pressure (with varying particle sizes) have clearly exhibited influence on the water infiltration process in all testing conditions. The numerical results of the distribution temperature, water infiltration, and infiltration depth are in agreement with the experimental results. The numerical results closely match with the experimental results obtained from S. Suttisong and P. Rattanadecho [17].
3. The water flux vectors near the surface of the packed bed are found to be higher than that of the infiltration front region. This is because the water saturation is higher near the surface of the packed bed, and at the infiltration front region where the water saturation is low.
4. The interplay between gravity force and water saturation impacts on water flux vectors, which are essential for numerical study of water infiltration process.

The idea behind this work can be used as guidance for special design of water flow in porous material processes in the future.

FUNDING

This work was supported by the Nation Research University Project of Thailand Office of Higher Education Commission and Thailand Research Fund.

REFERENCES

1. F. Stauffer and T. Dracos, Experimental and Numerical Study of Water and Solute Infiltration in Layered Porous Media, *J. of Hydrology*, vol. 84, pp. 9–34, 1986.
2. R. Haverkamp, M. Vauclin, J. Touma, P. J. Wierenga, and G. Vanchaud, A Comparison of Numerical Simulation Models for One-Dimensional Infiltration, *Soil Sci. Soc. Am. J.*, vol. 41, pp. 285–294, 1977.
3. J. Y. Parlange, Theory of Water Movement in Soils: One-Dimensional Infiltration, *Soil Science*, vol. 111, pp. 170–174, 1972.
4. B. A. Scherfler and Z. Xiaoyong, A Fully Coupled Model for a Water Flow and Air Flow in Deformable Porous Media, *Water Resources Research*, vol. 29, pp. 155–167, 1993.
5. H. Gvirtzman, E. Shalev, O. Dahan, and Y. H. Hatzor, Large-Scale Infiltration Experiments into Unsaturated Stratified Loess Sediment: Monitoring and Modeling, *Int. J. of Hydrology*, vol. 349, pp. 214–229, 2008.

6. J. T. Kulongoski and J. A. Izbicki, Simulation of Fluid Heat Transport to Estimate Desert Stream Infiltration, *Ground Water*, vol. 46, pp. 462–474, 2008.
7. Z. Xiuqing, M. W. Van Liew, and G. N. Flerchinger, Experimental Study of Infiltration into a Bean Stubble Field During Seasonal Freeze-Thaw Period, *Soil Science*, vol. 166, pp. 3–10, 2001.
8. M. Abriola and F. Pinder, A Multiphase Approach to the Modeling of Porous Media Contamination by Organic Compounds, 1. Equation development, *Water Resources Research*, vol. 21, pp. 11–18, 1985.
9. P. Binning and M. A. Celia, Practical Implementation of the Fractional Flow Approach to Multi-Phase Flow Simulation, *Int. J. Adva. in Water Resources*, vol. 22, pp. 461–478, 1999.
10. P. Ratanadecho, K. Aoki, and M. Akahori, Experimental and Numerical Study of Microwave Drying in Unsaturated Porous Material, *Int. Comm. in Heat and Mass Transfer*, vol. 28, pp. 605–616, 2001.
11. Y. Ma, S. Feng, D. Su, G. Gao, and Z. Huo, Modeling Water Infiltration in a Large Layered Soil Column with a Modified Green-Ampt Model, and HYDRUS-1D, *Int. J. Computer and Electronics in Agriculture*, vol. 71S, pp. S40–S47, 2010.
12. E. J. Henry and J. E. Smith, Numerical Demonstration of Surfactant Concentration-Dependent Capillarity and Viscosity Effects on Infiltration from a Constant Flux Line Source, *Int. J. of Hydrology*, vol. 329, pp. 63–74, 2006.
13. J. H. Eric and E. S. Jame, Numerical Demonstration of Surfactant Consentration-Dependent Capillarity and Viscosity Effects on Infiltration from a Constant Flux Line Source, *Int. J. of Hydrology*, vol. 329, pp. 63–74, 2006.
14. W. Quan-Jiu, R. Horton, and F. Jun, An Analytical Solution for One-Dimensional Water Infiltration and Redistribution in Unsaturated Soil, *Int. J. Pedosphere*, vol. 19, pp. 104–110, 2009.
15. K. Aoki, M. Hattori, M. Kitamura, and N. Shiraishi, Characteristics of Heat Transport in Porous Media with Water Infiltration, *ASME/JSME Thermal Eng. Proceeding*, vol. 4, pp. 303–308, 1991.
16. P. Ratanadecho, K. Aoki, and M. Akahori, Influence of Irradiation Time, Particle Sizes and Initial Moisture Content during Microwave Drying of Multi-Layered Capillary Porous Materials, *ASME J. Heat Transfer*, vol. 124, pp. 151–161, 2002.
17. S. Suttisong and P. Rattanadecho, The Experimental Investigation of Heat Transport, and Water Infiltration in Granular Packed Bed Due to Supplied Hot Water from the Top: Influence of Supplied Water Flux, Particle Sizes and Supplied Water Temperature, *Exp. Them. Fluid Sci.*, vol. 35, pp. 1530–1534, 2011.
18. I. Fayssal and F. Moukalled, A New Numerical Approach for Predicting the Two-Phase Flow of Refrigerants during Evaporation and Condensation, *Numer. Heat Transfer B*, vol. 62, pp. 341–369, 2012.
19. G. Yu, B. Yu, S. Sun, and W. Q. Tao, Comparative Study on Triangular and Quadrilateral Meshes by a Finite-Volume Method with a Central Difference Scheme, *Numer. Heat Transfer B*, vol. 62, pp. 243–263, 2012.
20. N. Georgios, Lygidakis, and K. Ioannis Nikolos, Using the Finite-Volume Method and Hybrid Unstructured Meshes to Compute Radiative Heat Transfer in 3-D Geometries, *Numer. Heat Transfer B*, vol. 62, pp. 289–314, 2012.
21. I. B. Celik, U. Ghia, P. J. Roache, C. J. Freias, H. W. Coleman, and P. E. Raad, Procedure for Estimation and Reporting of Uncertainty Due to Dicrestization in CFD Application, *J. Fluids Eng.—Trans. ASME*, vol. 130, pp. 078001, 2008.
22. T. Xing and F. Stern, Factors of Safety for Richardson Extrapolation, *J. Fluids Eng.—Trans. ASME*, vol. 132, pp. 061403–1, 2010.